NSS
Neutrosophic Sets and Systems, Vol. 75, 2025
University of New Mexico

Enhanced TFNN-GRA Technique for Multiple-Attribute Decision-Making with Triangular Fuzzy Neutrosophic Information and Applications to Performance Evaluation of Internally Cured High-Strength Concrete

Huayang Sun, Zhongyu Liu*

Zhengzhou University, Zhengzhou, 450001, Henan, China

*Corresponding author, E-mail: m18943699056@163.com

Abstract: Internal curing technology involves the integration of internal curing materials into concrete, typically under pre-water storage conditions. This method works by gradually releasing water to increase the internal humidity of the concrete, which enhances the hydration of cementitious materials, reduces self-shrinkage in high-strength concrete (HSC), and improves its overall performance. Commonly used internal curing materials include absorbent resin and lightweight aggregates. However, using these materials in excessive amounts can compromise the strength or durability of the concrete, making it essential to determine the optimal dosage for effective application. When applied to HSC, internal curing helps mitigate shrinkage and enhances frost resistance. As noted, accurately determining the appropriate dosage of internal curing materials is critical to maximizing these benefits. The performance evaluation of internally cured HSC is a multiple-attribute decision-making (MADM) problem, and to address the uncertainties involved in this process, triangular fuzzy neutrosophic sets (TFNSs) are particularly suitable. TFNSs offer a more precise way to represent uncertain information. Grey relational analysis (GRA), a widely used technique in grey system theory, assesses the similarity between sequence curves based on their geometric shapes. In this paper, we introduce a triangular fuzzy neutrosophic number GRA (TFNN-GRA) technique under TFNSs, where no prior weight information is available. Weight values under TFNSs are determined using information entropy. By combining GRA with TFNSs, we propose the TFNN-GRA method and outline the steps for solving MADM problems. Finally, a numerical example is presented to demonstrate the performance evaluation of internally cured HSC, along with comparative studies that highlight the advantages of the TFNN-GRA technique.

Keywords: Multiple-attribute decision-making (MAGM); TFNSs; GRA technique; performance evaluation of internally cured HSC

1. Introduction

HSC typically utilizes a low water-cement ratio and a high content of cementitious materials, making it denser than ordinary concrete and providing superior durability [1, 2]. As a result, it is often

recommended for outdoor structures exposed to seawater erosion, super-tall or large-span buildings, as well as engineering projects prone to impact damage. HSC is especially prevalent in infrastructure projects, where its ability to support large spans and heavy loads in harsh environments is highly valued [3, 4]. In China, high-strength self-compacting concrete is also widely used in steel-concrete composite columns for super high-rise buildings, as well as in other critical projects[5-7]. However, HSC is prone to early-stage cracking, which has become a significant focus of research within engineering and academic communities. Although admixtures like silica fume and ultrafine mineral powder are used to improve workability, they can also bring negative effects [8-10]. During both the early and later stages of curing, HSC requires more water to hydrate the large amounts of admixtures, which exacerbates self-shrinkage. Moreover, the elastic modulus of HSC is significantly higher than that of lower-strength concrete. This means that, even at the same shrinkage rate, HSC experiences much greater tensile stress without a corresponding increase in tensile strength, making it more susceptible to early cracking. Once cracks occur, the durability of HSC is compromised. High-performance concrete is well-suited for harsh environments and large-span structures [11, 12]. However, due to its low water-cement ratio, there is insufficient internal moisture to meet hydration requirements. Under normal curing conditions, its dense structure makes it difficult for external water to penetrate. As hydration progresses, this leads to self-shrinkage, which can cause cracks and diminish performance. While methods such as steam curing exist, they are expensive and often ineffective [13, 14]. After years of experimental research, it has been found that adding a certain proportion of internal curing materials can significantly reduce self-shrinkage, improve strength, and enhance the durability of high-performance concrete, achieving the desired results. There are two primary methods of curing concrete: internal curing and external curing[15, 16]. Initially, only external curing methods were used. However, with the development of concrete technology, HSC with a compressive strength of 100 MPa was first introduced in the 1940s. Despite its advantages, the low water-cement ratio of HSC causes shrinkage and cracking. The fundamental requirement for internal curing using lightweight aggregates is that the material must be porous and capable of retaining water. Common lightweight aggregates used internationally include ceramic particles, expanded shale, diatomaceous earth, and zeolites. Prior to being added to concrete, these aggregates

are pre-saturated with water. As the hydration of cementitious materials progresses, the moisture within the concrete decreases. Due to differences in humidity and capillary pressure, the water stored in the lightweight aggregates is slowly released, creating an optimal environment for the continued hydration of the cementitious materials [17]. However, it is important to note that the capillary water supply only occurs when the distance between the cement paste and the lightweight aggregate, known as the capillary pore distance, is between 100-200 μm. The effect is limited to this range. High water-absorbent resin (also known as superabsorbent polymer, or SAP) is another widely used internal curing material. This polymer has a complex, interwoven internal structure, containing a large number of hydrophilic groups such as carboxyl and hydroxyl groups. Its three-dimensional network of chemical chains allows it to absorb water at a rate thousands of times its own weight[18]. Because of its exceptional water retention properties at room temperature, high water-absorbent resin is more effective in maintaining moisture than lightweight aggregates. The typical particle size of SAP ranges from 100 to 250 μm. There are various types of SAP, including natural starch and cellulose, synthetic polyacrylic acid resin, polyacrylamide resin, acrylamide-acrylic acid copolymer, and hydroxyethyl cellulose ether. These materials are commonly produced using either dissolution or suspension polymerization methods [19]. Like lightweight aggregates, the purpose of using high water-absorbent resin in concrete is to provide an internal humidity environment that supports the ongoing hydration of cementitious materials. However, unlike lightweight aggregates, the release of water from SAP is not only driven by differences in humidity and capillary pressure but is also influenced by factors such as rising temperature and pH levels as the hydration process continues. Due to its superior water retention properties, SAP is often more suitable for concrete preparation than lightweight aggregates.

MADM plays a critical role in contemporary human society. In today's democratic and open social environments, its applications extend from purchasing essential household items and selecting corporate investment projects to determining locations for logistics distribution centers [20, 21]. These decision-making scenarios cover a wide range of sectors, involving varying scales of decision-makers, from a few family members to thousands of individuals. Well-informed decisions contribute to the growth and success of families, businesses, and even nations, whereas poor decisions can hinder

progress and lead to adverse consequences [22-24]. As society, the economy, and technology continue to evolve, the decision-making landscape grows more intricate, with increasingly diverse evaluation criteria for decision problems. Often, these criteria can be conflicting or restrictive with respect to one another. A critical challenge that scholars face is how to accurately represent the preference information of decision-makers. Due to the pressures of limited time, the complexity of decision-making tasks, and gaps in decision-makers' expertise, the preference information provided for alternative options tends to be vague. Traditional mathematical models, based on precise data, fail to capture this uncertainty [25, 26]. In response, various fuzzy set theories have been introduced by scholars globally, including fuzzy sets [27], single-valued neutrosophic sets (SVNSs) [28-30], and interval-valued neutrosophic sets (IVNSs) [31, 32]. These theories have been continuously refined, allowing for more accurate representations of decision-makers' fuzzy preferences. As such, efficiently aggregating uncertain information has become a key research focus in the realm of fuzzy MADM. In this study, the performance evaluation of internally cured HSC is considered as an example of MADM. TFNSs [33] are better suited for representing uncertainty in this context. Meanwhile, GRA [34] is utilized to assess the relational degree between sequences based on the geometric similarity of their curves. However, current methods related to the modified GRA technique [35, 36] within TFNNs are lacking. Therefore, it is crucial to integrate the TFNN-GRA approach into this context. The primary goal of this study is to develop the TFNN-GRA technique to enhance the MADM process. A numerical example involving the performance evaluation of internally cured HSC is provided, along with several comparative analyses to demonstrate the technique's effectiveness. The study's research objectives are as follows: (1) proposing the TFNN-GRA approach for MADM with TFNSs under completely unknown weights; (2) applying the entropy method to determine the weights within TFNSs; (3) utilizing the TFNN-GRA for performance evaluation of internally cured HSC; and (4) conducting comparative studies to verify that the TFNN-GRA technique is effective for this application.

To achieve this, the research framework is structured: Section 2 introduces the TFNNs. Section 3 presents the TFNN-GRA technique for MADM. In Section 4, numerical example is demonstrated the

application of TFNN-GRA technique in the performance evaluation of internally cured HSC. Section 5 offers the conclusions.

2. Preliminaries

Biswas et al. [33] constructed the TFNSs.

Definition 1[33]. The TFNSs UU is put forward:

$$UU=\left\{\left(\theta,UA(\theta),UB(\theta),UC(\theta)\right)\middle|\theta\in\Theta\right\} \tag{1}$$

where $UA(\theta),UB(\theta),UC(\theta)\in[0,1]$ is truth-membership, indeterminacy-membership and falsity-membership by TFNs.

$$UA(\theta)=\left(UA^{L}(\theta),UA^{M}(\theta),UA^{U}(\theta)\right),0\le UA^{L}(\theta)\le UA^{M}(\theta)\le UA^{U}(\theta)\le 1 \tag{2}$$

$$UB(\theta)=\left(UB^{L}(\theta),UB^{M}(\theta),UB^{U}(\theta)\right),0\le UB^{L}(\theta)\le UB^{M}(\theta)\le UB^{U}(\theta)\le 1 \tag{3}$$

$$UC(\theta)=\left(UC^{L}(\theta),UC^{M}(\theta),UC^{U}(\theta)\right),0\le UC^{L}(\theta)\le UC^{M}(\theta)\le UC^{U}(\theta)\le 1 \tag{4}$$

For convenience, $UU=\left\{\left(UA^{L},UA^{M},UA^{U}\right),\left(UB^{L},UB^{M},UB^{U}\right),\left(UC^{L},UC^{M},UC^{U}\right)\right\}$ is TFNN, and meet $0\le UA^{U}+UB^{U}+UC^{U}\le 3$.

Definition 2[33]. Let $UU_1=\left\{\left(UA_1^{L},UA_1^{M},UA_1^{U}\right),\left(UB_1^{L},UB_1^{M},UB_1^{U}\right),\left(UC_1^{L},UC_1^{M},UC_1^{U}\right)\right\}$, $UU_2=\left\{\left(UA_2^{L},UA_2^{M},UA_2^{U}\right),\left(UB_2^{L},UB_2^{M},UB_2^{U}\right),\left(UC_2^{L},UC_2^{M},UC_2^{U}\right)\right\}$ and $UU=\left\{\left(UA^{L},UA^{M},UA^{U}\right),\left(UB^{L},UB^{M},UB^{U}\right),\left(UC^{L},UC^{M},UC^{U}\right)\right\}$, the operational laws are put forward:

$$(1)\ UU_1 \oplus UU_2 = \left\{ \begin{pmatrix} UA_1^L + UA_2^L - UA_1^L UA_2^L, \\ UA_1^M + UA_2^M - UA_1^M UA_2^M, UA_1^U + UA_2^U - UA_1^U UA_2^U \end{pmatrix}, \right.$$
$$\left. \left(UB_1^L UB_2^L, UB_1^M UB_2^M, UB_1^U UB_2^U\right), \left(UC_1^L UC_2^L, UC_1^M UC_2^M, UC_1^U UC_2^U\right) \right\};$$

$$(2)\ UU_1 \otimes UU_2 = \left\{ \left(UA_1^L UA_2^L, UA_1^M UA_2^M, UA_1^U UA_2^U\right), \right.$$
$$\begin{pmatrix} UB_1^L + UB_2^L - UB_1^L UB_2^L, \\ UB_1^M + UB_2^M - UB_1^M UB_2^M, UB_1^U + UB_2^U - UB_1^U UB_2^U \end{pmatrix},$$
$$\left. \begin{pmatrix} UC_1^L + UC_2^L - UC_1^L UC_2^L, \\ UC_1^M + UC_2^M - UC_1^M UC_2^M, UC_1^U + UC_2^U - UC_1^U UC_2^U \end{pmatrix} \right\};$$

$$(3)\ \xi UU = \left\{ \begin{pmatrix} 1-\left(1-UA^L\right)^\xi, 1-\left(1-UA^M\right)^\xi, 1-\left(1-UA^U\right)^\xi \end{pmatrix}, \right.$$
$$\left(\left(UB^L\right)^\xi, \left(UB^M\right)^\xi, \left(UB^U\right)^\xi \right),$$
$$\left. \left(\left(UC^L\right)^\xi, \left(UC^M\right)^\xi, \left(UC^U\right)^\xi \right) \right\}, \xi > 0;$$

$$(4)\ UU^\xi = \left\{ \left(\left(UA^L\right)^\xi, \left(UA^M\right)^\xi, \left(UA^U\right)^\xi \right), \right.$$
$$\left(1-\left(1-UB^L\right)^\xi, 1-\left(1-UB^M\right)^\xi, 1-\left(1-UB^U\right)^\xi \right),$$
$$\left. \left(1-\left(1-UC^L\right)^\xi, 1-\left(1-UC^M\right)^\xi, 1-\left(1-UC^U\right)^\xi \right) \right\}, \xi > 0.$$

Through Definition 2, serval properties are constructed.

$$(1)\ UU_1 \oplus UU_2 = UU_2 \oplus UU_1, UU_1 \otimes UU_2 = UU_2 \otimes UU_1, \left(\left(UU_1\right)^{\xi_1} \right)^{\xi_2} = \left(UU_1\right)^{\xi_1 \xi_2}; \quad (5)$$

$$(2)\ \xi\left(UU_1 \oplus UU_2\right) = \xi UU_1 \oplus \xi UU_2, \left(UU_1 \otimes UU_2\right)^\xi = \left(UU_1\right)^\xi \otimes \left(UU_2\right)^\xi; \quad (6)$$

$$(3) \xi_1 UU_1 \oplus \xi_2 UU_1 = \left(\xi_1 + \xi_2\right) UU_1, \left(UU_1\right)^{\xi_1} \otimes \left(UU_1\right)^{\xi_2} = \left(UU_1\right)^{\left(\xi_1 + \xi_2\right)}. \quad (7)$$

Definition 3[33]. Let $UU = \left\{ \left(UA^L, UA^M, UA^U\right), \left(UB^L, UB^M, UB^U\right), \left(UC^L, UC^M, UC^U\right) \right\}$, the score functions (SF) and accuracy functions (AF) are constructed:

$$SF\left(UU\right)=\frac{1}{12}\begin{bmatrix}8+\left(UA^{L}+2UA^{M}+UA^{U}\right)\\-\left(UB^{L}+2UB^{M}+UB^{U}\right)\\-\left(UC^{L}+2UC^{M}+UC^{U}\right)\end{bmatrix},SF\left(UU\right)\in\left[0,1\right] \tag{8}$$

$$AF\left(UU\right)=\frac{1}{8}\begin{bmatrix}4+\left(UA^{L}+2UA^{M}+UA^{U}\right)\\-\left(UB^{L}+2UB^{M}+UB^{U}\right)\end{bmatrix},AF\left(UU\right)\in\left[0,1\right] \tag{9}$$

For two TFNNs UU_1 and UU_2, then

(1) *if* $SF\left(UU_1\right)\prec SF\left(UU_2\right),\ UU_1\prec UU_2$;
(2) *if* $SF\left(UU_1\right)=SF\left(UU_2\right),AF\left(UU_1\right)\prec AF\left(UU_2\right),UU_1\prec UU_2$;
(3) *if* $SF\left(UU_1\right)=SF\left(UU_2\right),AF\left(UU_1\right)=AF\left(UU_2\right),UU_1=UU_2$.

Definition 4[37]. Let $UU_1=\left\{\left(UA_1^L,UA_1^M,UA_1^U\right),\left(UB_1^L,UB_1^M,UB_1^U\right),\left(UC_1^L,UC_1^M,UC_1^U\right)\right\}$, $UU_2=\left\{\left(UA_2^L,UA_2^M,UA_2^U\right),\left(UB_2^L,UB_2^M,UB_2^U\right),\left(UC_2^L,UC_2^M,UC_2^U\right)\right\}$, the mixed distance is put forward based on the Euclidean distance and Hamming distance:

$$\begin{aligned}&MD\left(UU_1,UU_2\right)=ED\left(UU_1,UU_2\right)+HD\left(UU_1,UU_2\right)\\&=\frac{1}{2}\left(\sqrt{\frac{1}{9}\left(\begin{array}{l}\left|UA_1^L-UA_2^L\right|^2+\left|UA_1^M-UA_2^M\right|^2+\left|UA_1^U-UA_2^U\right|^2\\+\left|UB_1^L-UB_2^L\right|^2+\left|UB_1^M-UB_2^M\right|^2+\left|UB_1^U-UB_2^U\right|^2\\+\left|UC_1^L-UC_2^L\right|^2+\left|UC_1^M-UC_2^M\right|^2+\left|UC_1^U-UC_2^U\right|^2\end{array}\right)}+\right.\\&\left.\frac{1}{9}\left(\begin{array}{l}\left|UA_1^L-UA_2^L\right|+\left|UA_1^M-UA_2^M\right|+\left|UA_1^U-UA_2^U\right|\\+\left|UB_1^L-UB_2^L\right|+\left|UB_1^M-UB_2^M\right|+\left|UB_1^U-UB_2^U\right|\\+\left|UC_1^L-UC_2^L\right|+\left|UC_1^M-UC_2^M\right|+\left|UC_1^U-UC_2^U\right|\end{array}\right)\right)\end{aligned} \tag{10}$$

3. GRA technique for MADM issue with TFNNs

The TFNN-GRA is put forward for MADM. There are m alternatives $\left\{UX_1,UX_2,\ldots,UX_m\right\}$, n devised attributes $\left\{UG_1,UG_2,\ldots,UG_n\right\}$ and TFNN-GRA technique for MADM are constructed (**Figure 1**).

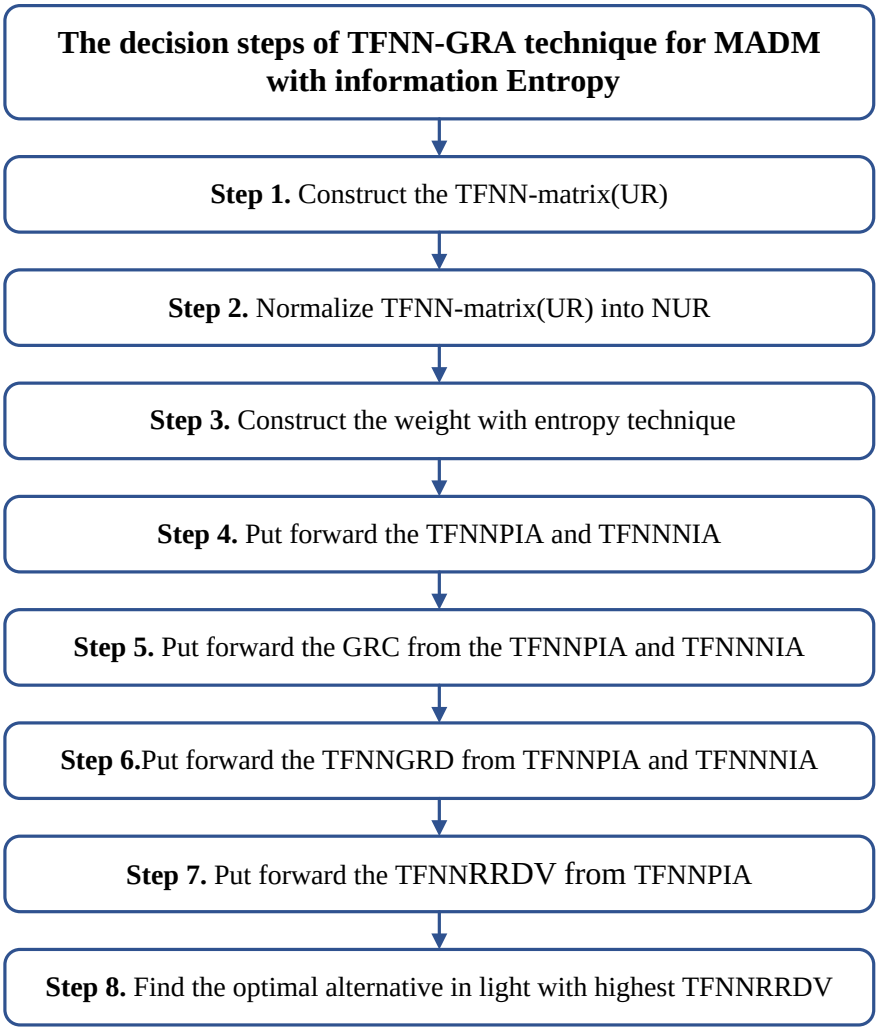

Figure 1. Framework of TFNN-GRA for MADM

Step 1. Construct the TFNN-matrix $UR = \left[UR_{ij} \right]_{m\times n}$:

$$UR = \left[UR_{ij} \right]_{m\times n} = \begin{array}{c} \\ UX_1 \\ UX_2 \\ \vdots \\ UX_m \end{array} \begin{array}{c} \begin{array}{cccc} UG_1 & UG_2 & \ldots & UG_n \end{array} \\ \begin{bmatrix} UR_{11} & UR_{12} & \ldots & UR_{1n} \\ UR_{21} & UR_{22} & \ldots & UR_{2n} \\ \vdots & \vdots & \vdots & \vdots \\ UR_{m1} & UR_{m2} & \ldots & UR_{mn} \end{bmatrix} \end{array} \tag{11}$$

where $UR_{ij} = \begin{Bmatrix} \left(\left(UA_{ij}^{L} \right), \left(UA_{ij}^{M} \right), \left(UA_{ij}^{U} \right) \right), \\ \left(\left(UB_{ij}^{L} \right), \left(UB_{ij}^{M} \right), \left(UB_{ij}^{U} \right) \right), \\ \left(\left(UC_{ij}^{L} \right), \left(UC_{ij}^{M} \right), \left(UC_{ij}^{U} \right) \right) \end{Bmatrix}$.

Step 2. Normalize the $UR = \left[UR_{ij} \right]_{m\times n}$ to $NUR = \left[NUR_{ij} \right]_{m\times n}$.

Aimed at benefit attributes:

$$NUR_{ij}=\begin{Bmatrix}\left(\left(NUA_{ij}^{L}\right),\left(NUA_{ij}^{M}\right),\left(NUA_{ij}^{U}\right)\right),\\ \left(\left(NUB_{ij}^{L}\right),\left(NUB_{ij}^{M}\right),\left(NUB_{ij}^{U}\right)\right),\\ \left(\left(NUC_{ij}^{L}\right),\left(NUC_{ij}^{M}\right),\left(NUC_{ij}^{U}\right)\right)\end{Bmatrix}=\begin{Bmatrix}\left(\left(UA_{ij}^{L}\right),\left(UA_{ij}^{M}\right),\left(UA_{ij}^{U}\right)\right),\\ \left(\left(UB_{ij}^{L}\right),\left(UB_{ij}^{M}\right),\left(UB_{ij}^{U}\right)\right),\\ \left(\left(UC_{ij}^{L}\right),\left(UC_{ij}^{M}\right),\left(UC_{ij}^{U}\right)\right)\end{Bmatrix} \tag{12}$$

Aimed at cost attributes:

$$NUR_{ij}=\begin{Bmatrix}\left(\left(NUA_{ij}^{L}\right),\left(NUA_{ij}^{M}\right),\left(NUA_{ij}^{U}\right)\right),\\ \left(\left(NUB_{ij}^{L}\right),\left(NUB_{ij}^{M}\right),\left(NUB_{ij}^{U}\right)\right),\\ \left(\left(NUC_{ij}^{L}\right),\left(NUC_{ij}^{M}\right),\left(NUC_{ij}^{U}\right)\right)\end{Bmatrix}=\begin{Bmatrix}\left(\left(UC_{ij}^{L}\right),\left(UC_{ij}^{M}\right),\left(UC_{ij}^{U}\right)\right),\\ \left(\left(UB_{ij}^{L}\right),\left(UB_{ij}^{M}\right),\left(UB_{ij}^{U}\right)\right),\\ \left(\left(UA_{ij}^{L}\right),\left(UA_{ij}^{M}\right),\left(UA_{ij}^{U}\right)\right)\end{Bmatrix} \tag{13}$$

Step 3. Obtain the weight with entropy technique.

Entropy [38] is a better technique to obtain weight. The normalized TFNN-matrix $NTFNN_{ij}$ is constructed:

$$NTFNN_{ij}=\frac{SF\begin{Bmatrix}\left(\left(NUA_{ij}^{L}\right),\left(NUA_{ij}^{M}\right),\left(NUA_{ij}^{U}\right)\right),\\ \left(\left(NUB_{ij}^{L}\right),\left(NUB_{ij}^{M}\right),\left(NUB_{ij}^{U}\right)\right),\\ \left(\left(NUC_{ij}^{L}\right),\left(NUC_{ij}^{M}\right),\left(NUC_{ij}^{U}\right)\right)\end{Bmatrix}+AF\begin{Bmatrix}\left(\left(NUA_{ij}^{L}\right),\left(NUA_{ij}^{M}\right),\left(NUA_{ij}^{U}\right)\right),\\ \left(\left(NUB_{ij}^{L}\right),\left(NUB_{ij}^{M}\right),\left(NUB_{ij}^{U}\right)\right),\\ \left(\left(NUC_{ij}^{L}\right),\left(NUC_{ij}^{M}\right),\left(NUC_{ij}^{U}\right)\right)\end{Bmatrix}+1}{\sum_{i=1}^{m}\left(SF\begin{Bmatrix}\left(\left(NUA_{ij}^{L}\right),\left(NUA_{ij}^{M}\right),\left(NUA_{ij}^{U}\right)\right),\\ \left(\left(NUB_{ij}^{L}\right),\left(NUB_{ij}^{M}\right),\left(NUB_{ij}^{U}\right)\right),\\ \left(\left(NUC_{ij}^{L}\right),\left(NUC_{ij}^{M}\right),\left(NUC_{ij}^{U}\right)\right)\end{Bmatrix}+AF\begin{Bmatrix}\left(\left(NUA_{ij}^{L}\right),\left(NUA_{ij}^{M}\right),\left(NUA_{ij}^{U}\right)\right),\\ \left(\left(NUB_{ij}^{L}\right),\left(NUB_{ij}^{M}\right),\left(NUB_{ij}^{U}\right)\right),\\ \left(\left(NUC_{ij}^{L}\right),\left(NUC_{ij}^{M}\right),\left(NUC_{ij}^{U}\right)\right)\end{Bmatrix}+1\right)}, \tag{14}$$

Then, TFNN Shannon decision entropy (TFNNSDE) is put forward through Eq. (15):

$$TFNNSDE_{j}=-\frac{1}{\ln m}\sum_{i=1}^{m}NTFNN_{ij}\ln NTFNN_{ij} \tag{15}$$

and $NTFNN_{ij}\ln NTFNN_{ij}=0$ if $NTFNN_{ij}=0$.

Then, the weights $UW=\left(UW_{1},UW_{2},\cdots,UW_{n}\right)$ is derived:

$$UW_j = \frac{1-TPNNSE_j}{\sum_{j=1}^{n}\left(1-TPNNSE_j\right)}, \quad j=1,2,\cdots,n. \tag{16}$$

Step 4. Put forward the TFNN positive ideal alternative (TFNNPIA) and TFNN negative ideal alternative (TFNNNIA)[39]:

$$TPNNPIA = \begin{Bmatrix} \left(\left(NUA_j^L\right)^+, \left(NUA_j^M\right)^+, \left(NUA_j^U\right)^+\right), \\ \left(\left(NUB_j^L\right)^+, \left(NUB_j^M\right)^+, \left(NUB_j^U\right)^+\right), \\ \left(\left(NUC_j^L\right)^+, \left(NUC_j^M\right)^+, \left(NUC_j^U\right)^+\right) \end{Bmatrix} \tag{17}$$

$$TFNNNIA = \begin{Bmatrix} \left(\left(NUA_j^L\right)^-, \left(NUA_j^M\right)^-, \left(NUA_j^U\right)^-\right), \\ \left(\left(NUB_j^L\right)^-, \left(NUB_j^M\right)^-, \left(NUB_j^U\right)^+\right), \\ \left(\left(NUC_j^L\right)^-, \left(NUC_j^M\right)^-, \left(NUC_j^U\right)^-\right) \end{Bmatrix} \tag{18}$$

$$\begin{aligned} &SF\begin{Bmatrix} \left(\left(NUA_j^L\right)^+, \left(NUA_j^M\right)^+, \left(NUA_j^U\right)^+\right), \\ \left(\left(NUB_j^L\right)^+, \left(NUB_j^M\right)^+, \left(NUB_j^U\right)^+\right), \\ \left(\left(NUC_j^L\right)^+, \left(NUC_j^M\right)^+, \left(NUC_j^U\right)^+\right) \end{Bmatrix} \\ &= \max_i SF\begin{Bmatrix} \left(\left(NUA_{ij}^L\right), \left(NUA_{ij}^M\right), \left(NUA_{ij}^U\right)\right), \\ \left(\left(NUB_{ij}^L\right), \left(NUB_{ij}^M\right), \left(NUB_{ij}^U\right)\right), \\ \left(\left(NUC_{ij}^L\right), \left(NUC_{ij}^M\right), \left(NUC_{ij}^U\right)\right) \end{Bmatrix} \end{aligned} \tag{19}$$

$$\begin{aligned} &SF\begin{Bmatrix} \left(\left(NUA_j^L\right)^-, \left(NUA_j^M\right)^-, \left(NUA_j^U\right)^-\right), \\ \left(\left(NUB_j^L\right)^-, \left(NUB_j^M\right)^-, \left(NUB_j^U\right)^+\right), \\ \left(\left(NUC_j^L\right)^-, \left(NUC_j^M\right)^-, \left(NUC_j^U\right)^-\right) \end{Bmatrix} \\ &= \min_i SF\begin{Bmatrix} \left(\left(NUA_{ij}^L\right), \left(NUA_{ij}^M\right), \left(NUA_{ij}^U\right)\right), \\ \left(\left(NUB_{ij}^L\right), \left(NUB_{ij}^M\right), \left(NUB_{ij}^U\right)\right), \\ \left(\left(NUC_{ij}^L\right), \left(NUC_{ij}^M\right), \left(NUC_{ij}^U\right)\right) \end{Bmatrix} \end{aligned} \tag{20}$$

Step 5. Put forward the grey rational coefficients (GRC) from TFNNPIA and TFNNNIA:

$$TFNNPIA\left(\xi_{ij}\right)=\frac{\left(\begin{array}{l}\min\limits_{1\le i\le m} MD\left(\left\{\begin{array}{l}\left(\left(NUA_j^L\right)^+,\left(NUA_j^M\right)^+,\left(NUA_j^U\right)^+\right),\\ \left(\left(NUB_j^L\right)^+,\left(NUB_j^M\right)^+,\left(NUB_j^U\right)^+\right),\\ \left(\left(NUC_j^L\right)^+,\left(NUC_j^M\right)^+,\left(NUC_j^U\right)^+\right)\end{array}\right\},\left\{\begin{array}{l}\left(\left(NUA_{ij}^L\right),\left(NUA_{ij}^M\right),\left(NUA_{ij}^U\right)\right),\\ \left(\left(NUB_{ij}^L\right),\left(NUB_{ij}^M\right),\left(NUB_{ij}^U\right)\right),\\ \left(\left(NUC_{ij}^L\right),\left(NUC_{ij}^M\right),\left(NUC_{ij}^U\right)\right)\end{array}\right\}\right)+\\ \rho\max\limits_{1\le i\le m} MD\left(\left\{\begin{array}{l}\left(\left(NUA_j^L\right)^+,\left(NUA_j^M\right)^+,\left(NUA_j^U\right)^+\right),\\ \left(\left(NUB_j^L\right)^+,\left(NUB_j^M\right)^+,\left(NUB_j^U\right)^+\right),\\ \left(\left(NUC_j^L\right)^+,\left(NUC_j^M\right)^+,\left(NUC_j^U\right)^+\right)\end{array}\right\},\left\{\begin{array}{l}\left(\left(NUA_{ij}^L\right),\left(NUA_{ij}^M\right),\left(NUA_{ij}^U\right)\right),\\ \left(\left(NUB_{ij}^L\right),\left(NUB_{ij}^M\right),\left(NUB_{ij}^U\right)\right),\\ \left(\left(NUC_{ij}^L\right),\left(NUC_{ij}^M\right),\left(NUC_{ij}^U\right)\right)\end{array}\right\}\right)\end{array}\right)}{\left(\begin{array}{l}MD\left(\left\{\begin{array}{l}\left(\left(NUA_j^L\right)^+,\left(NUA_j^M\right)^+,\left(NUA_j^U\right)^+\right),\\ \left(\left(NUB_j^L\right)^+,\left(NUB_j^M\right)^+,\left(NUB_j^U\right)^+\right),\\ \left(\left(NUC_j^L\right)^+,\left(NUC_j^M\right)^+,\left(NUC_j^U\right)^+\right)\end{array}\right\},\left\{\begin{array}{l}\left(\left(NUA_{ij}^L\right),\left(NUA_{ij}^M\right),\left(NUA_{ij}^U\right)\right),\\ \left(\left(NUB_{ij}^L\right),\left(NUB_{ij}^M\right),\left(NUB_{ij}^U\right)\right),\\ \left(\left(NUC_{ij}^L\right),\left(NUC_{ij}^M\right),\left(NUC_{ij}^U\right)\right)\end{array}\right\}\right)\\ +\rho\max\limits_{1\le i\le m} MD\left(\left\{\begin{array}{l}\left(\left(NUA_j^L\right)^+,\left(NUA_j^M\right)^+,\left(NUA_j^U\right)^+\right),\\ \left(\left(NUB_j^L\right)^+,\left(NUB_j^M\right)^+,\left(NUB_j^U\right)^+\right),\\ \left(\left(NUC_j^L\right)^+,\left(NUC_j^M\right)^+,\left(NUC_j^U\right)^+\right)\end{array}\right\},\left\{\begin{array}{l}\left(\left(NUA_{ij}^L\right),\left(NUA_{ij}^M\right),\left(NUA_{ij}^U\right)\right),\\ \left(\left(NUB_{ij}^L\right),\left(NUB_{ij}^M\right),\left(NUB_{ij}^U\right)\right),\\ \left(\left(NUC_{ij}^L\right),\left(NUC_{ij}^M\right),\left(NUC_{ij}^U\right)\right)\end{array}\right\}\right)\end{array}\right)} \tag{21}$$

$$TFNNNIA\left(\xi_{ij}\right)=\frac{\left(\begin{array}{l}\min\limits_{1\le i\le m} MD\left(\left\{\begin{array}{l}\left(\left(NUA_j^L\right)^-,\left(NUA_j^M\right)^-,\left(NUA_j^U\right)^-\right),\\ \left(\left(NUB_j^L\right)^-,\left(NUB_j^M\right)^-,\left(NUB_j^U\right)^+\right),\\ \left(\left(NUC_j^L\right)^-,\left(NUC_j^M\right)^-,\left(NUC_j^U\right)^-\right)\end{array}\right\},\left\{\begin{array}{l}\left(\left(NUA_{ij}^L\right),\left(NUA_{ij}^M\right),\left(NUA_{ij}^U\right)\right),\\ \left(\left(NUB_{ij}^L\right),\left(NUB_{ij}^M\right),\left(NUB_{ij}^U\right)\right),\\ \left(\left(NUC_{ij}^L\right),\left(NUC_{ij}^M\right),\left(NUC_{ij}^U\right)\right)\end{array}\right\}\right)+\\ \rho\max\limits_{1\le i\le m} MD\left(\left\{\begin{array}{l}\left(\left(NPA_j^L\right)^-,\left(NPA_j^M\right)^-,\left(NPA_j^U\right)^-\right),\\ \left(\left(NPB_j^L\right)^-,\left(NPB_j^M\right)^-,\left(NPB_j^U\right)^+\right),\\ \left(\left(NPC_j^L\right)^-,\left(NPC_j^M\right)^-,\left(NPC_j^U\right)^-\right)\end{array}\right\},\left\{\begin{array}{l}\left(\left(NPA_{ij}^L\right),\left(NPA_{ij}^M\right),\left(NPA_{ij}^U\right)\right),\\ \left(\left(NPB_{ij}^L\right),\left(NPB_{ij}^M\right),\left(NPB_{ij}^U\right)\right),\\ \left(\left(NPC_{ij}^L\right),\left(NPC_{ij}^M\right),\left(NPC_{ij}^U\right)\right)\end{array}\right\}\right)\end{array}\right)}{\left(\begin{array}{l}MD\left(\left\{\begin{array}{l}\left(\left(NUA_j^L\right)^-,\left(NUA_j^M\right)^-,\left(NUA_j^U\right)^-\right),\\ \left(\left(NUB_j^L\right)^-,\left(NUB_j^M\right)^-,\left(NUB_j^U\right)^+\right),\\ \left(\left(NUC_j^L\right)^-,\left(NUC_j^M\right)^-,\left(NUC_j^U\right)^-\right)\end{array}\right\},\left\{\begin{array}{l}\left(\left(NUA_{ij}^L\right),\left(NUA_{ij}^M\right),\left(NUA_{ij}^U\right)\right),\\ \left(\left(NUB_{ij}^L\right),\left(NUB_{ij}^M\right),\left(NUB_{ij}^U\right)\right),\\ \left(\left(NUC_{ij}^L\right),\left(NUC_{ij}^M\right),\left(NUC_{ij}^U\right)\right)\end{array}\right\}\right)\\ +\rho\max\limits_{1\le i\le m} MD\left(\left\{\begin{array}{l}\left(\left(NPA_j^L\right)^-,\left(NPA_j^M\right)^-,\left(NPA_j^U\right)^-\right),\\ \left(\left(NPB_j^L\right)^-,\left(NPB_j^M\right)^-,\left(NPB_j^U\right)^+\right),\\ \left(\left(NPC_j^L\right)^-,\left(NPC_j^M\right)^-,\left(NPC_j^U\right)^-\right)\end{array}\right\},\left\{\begin{array}{l}\left(\left(NPA_{ij}^L\right),\left(NPA_{ij}^M\right),\left(NPA_{ij}^U\right)\right),\\ \left(\left(NPB_{ij}^L\right),\left(NPB_{ij}^M\right),\left(NPB_{ij}^U\right)\right),\\ \left(\left(NPC_{ij}^L\right),\left(NPC_{ij}^M\right),\left(NPC_{ij}^U\right)\right)\end{array}\right\}\right)\end{array}\right)} \tag{22}$$

The distinguishing coefficient ρ =0.5.

Step 6. Put forward the TFNN grey relation degree (TFNNGRD) from TFNNPIA and TFNNNIA:

$$TFNNGRD\left(\xi_i^+\right)=\sum_{j=1}^{n} UW_j\times TFNNPIA\left(\xi_{ij}\right) \tag{23}$$

$$TFNNGRD\left(\xi_i^-\right)=\sum_{j=1}^{n} UW_j\times TFNNNIA\left(\xi_{ij}\right) \tag{24}$$

Step 7. Put forward the TFNN relative relational degree values (TFNNRRDV) from TFNNPIA:

$$\begin{aligned} TFNNRRDV\left(\xi_i\right)&=\frac{TFNNGRD\left(\xi_i^+\right)}{TFNNGRD\left(\xi_i^-\right)+TFNNGRD\left(\xi_i^+\right)}\\ &=\frac{\sum_{j=1}^{n} UW_j\times TFNNPIA\left(\xi_{ij}\right)}{\sum_{j=1}^{n} UW_j\times TFNNPIA\left(\xi_{ij}\right)+\sum_{j=1}^{n} UW_j\times TFNNNIA\left(\xi_{ij}\right)} \end{aligned} \tag{25}$$

Step 8. Find the optimal alternative in light with highest $TFNNRRDV\left(\xi_i\right)$.

4. Numerical example and comparative analysis

4.1. Numerical example

HSC is known for its early cracking and unstable volume shape, which significantly impact its durability. Among the factors causing cracks, only about 20% are due to external loads. The majority of structural cracks in HSC occur after the initial setting and are primarily due to changes in self-generated volume and external environmental influences. HSC has a higher density than ordinary concrete, but its low water-cement ratio results in lower porosity. This characteristic suggests that incorporating internal curing materials in HSC can effectively reduce crack formation and mitigate cracking. Internal curing materials, such as high-water absorbent resin, play a crucial role in this process. These materials have a strong water absorption capacity. When mixed with HSC, the high-water absorbent resin absorbs free water during the early stages of concrete hydration, preventing its loss. As the hydration process progresses and the hydration storage capacity decreases, the resin releases the absorbed water, allowing hydration to continue. This mechanism is particularly beneficial for HSC, which has a lower water-cement ratio compared to ordinary concrete. The primary cause of self-shrinkage in HSC is the change in internal humidity. The introduction of internal curing materials like Super Absorbent Polymers (SAP) can effectively address this issue by alleviating the drying problem inside the concrete during hydration. SAP absorbs excess water and releases it as needed, ensuring continuous hydration and reducing self-shrinkage. This internal curing method helps to control crack formation more effectively in HSC than in ordinary concrete, enhancing its overall durability and structural integrity. In summary, the use of internal curing materials in HSC is a promising approach to mitigate early cracking and unstable volume changes.

By managing internal humidity and supporting continuous hydration, these materials help to reduce self-shrinkage and improve the durability of HSC. The performance evaluation of internally cured HSC is MADM. Numerical example for performance evaluation of internally cured HSC based on TFNN-GRA. Five internally cured HSCs $UX_i\left(i=1,2,3,4,5\right)$ are evaluated with four attributes: ①UG_1 is compressive strength; ②UG_2 is the mass loss rate; ③UG_3 is relative dynamic modulus of elasticity; ④UG_4 is self-shrinkage shrinkage rate. The five internally cured HSCs $UX_i\left(i=1,2,3,4,5\right)$ are evaluated with four attributes through employing the TFNNs. The TFNN-GRA technique is used for performance evaluation of internally cured HSC.

Step 1. Put forward the TFNN-matrix $UR=\left[UR_{ij}\right]_{m\times n}$ (See Table 1).

Table 1. The TFNN data

	PG_1	PG_2
PX_1	$\begin{Bmatrix}(0.51,0.65,0.76),\\(0.59,0.81,0.87),\\(0.46,0.63,0.72)\end{Bmatrix}$	$\begin{Bmatrix}(0.57,0.63,0.69),\\(0.57,0.61,0.72),\\(0.36,0.42,0.54)\end{Bmatrix}$
PX_2	$\begin{Bmatrix}(0.63,0.68,0.73),\\(0.47,0.53,0.64),\\(0.36,0.42,0.56)\end{Bmatrix}$	$\begin{Bmatrix}(0.53,0.65,0.69),\\(0.34,0.42,0.57),\\(0.26,0.32,0.45)\end{Bmatrix}$
PX_3	$\begin{Bmatrix}(0.63,0.76,0.84),\\(0.48,0.53,0.64),\\(0.59,0.67,0.72)\end{Bmatrix}$	$\begin{Bmatrix}(0.48,0.52,0.85),\\(0.25,0.56,0.67),\\(0.31,0.43,0.74)\end{Bmatrix}$
PX_4	$\begin{Bmatrix}(0.54,0.68,0.74),\\(0.34,0.57,0.63),\\(0.46,0.63,0.72)\end{Bmatrix}$	$\begin{Bmatrix}(0.43,0.62,0.71),\\(0.54,0.68,0.79),\\(0.45,0.54,0.63)\end{Bmatrix}$
PX_5	$\begin{Bmatrix}(0.53,0.69,0.81),\\(0.64,0.72,0.76),\\(0.45,0.58,0.74)\end{Bmatrix}$	$\begin{Bmatrix}(0.34,0.53,0.76),\\(0.39,0.48,0.56),\\(0.32,0.45,0.64)\end{Bmatrix}$

	PG_3	PG_4
PX_1	$\begin{Bmatrix}(0.53,0.61,0.76),\\(0.42,0.54,0.65),\\(0.74,0.81,0.86)\end{Bmatrix}$	$\begin{Bmatrix}(0.28,0.43,0.67),\\(0.34,0.58,0.89),\\(0.63,0.75,0.83)\end{Bmatrix}$
PX_2	$\begin{Bmatrix}(0.43,0.57,0.84),\\(0.46,0.51,0.62),\\(0.37,0.43,0.57)\end{Bmatrix}$	$\begin{Bmatrix}(0.31,0.42,0.46),\\(0.54,0.65,0.74),\\(0.56,0.64,0.83)\end{Bmatrix}$
PX_3	$\begin{Bmatrix}(0.62,0.74,0.86),\\(0.29,0.56,0.69),\\(0.39,0.46,0.76)\end{Bmatrix}$	$\begin{Bmatrix}(0.73,0.76,0.82),\\(0.57,0.68,0.75),\\(0.43,0.56,0.62)\end{Bmatrix}$
PX_4	$\begin{Bmatrix}(0.63,0.84,0.89),\\(0.23,0.38,0.57),\\(0.28,0.36,0.46)\end{Bmatrix}$	$\begin{Bmatrix}(0.35,0.52,0.73),\\(0.67,0.73,0.78),\\(0.29,0.34,0.45)\end{Bmatrix}$
PX_5	$\begin{Bmatrix}(0.57,0.62,0.71),\\(0.46,0.53,0.67),\\(0.53,0.62,0.74)\end{Bmatrix}$	$\begin{Bmatrix}(0.43,0.52,0.63),\\(0.36,0.46,0.54),\\(0.48,0.52,0.63)\end{Bmatrix}$

Step 2. Normalize the $UR=\left[UR_{ij}\right]_{5\times4}$ to $NUR=\left[NUR_{ij}\right]_{5\times4}$. All the attributes are benefit, the $NUR=\left[NUR_{ij}\right]_{5\times4}$ is same to $UR=\left[UR_{ij}\right]_{5\times4}$ (See Table 2).

Table 2. The normalized TFNN data

	PG_1	PG_2
PX_1	$\begin{Bmatrix}(0.51,0.65,0.76),\\(0.59,0.81,0.87),\\(0.46,0.63,0.72)\end{Bmatrix}$	$\begin{Bmatrix}(0.57,0.63,0.69),\\(0.57,0.61,0.72),\\(0.36,0.42,0.54)\end{Bmatrix}$
PX_2	$\begin{Bmatrix}(0.63,0.68,0.73),\\(0.47,0.53,0.64),\\(0.36,0.42,0.56)\end{Bmatrix}$	$\begin{Bmatrix}(0.53,0.65,0.69),\\(0.34,0.42,0.57),\\(0.26,0.32,0.45)\end{Bmatrix}$

PX_3	$\begin{Bmatrix}(0.63,0.76,0.84),\\(0.48,0.53,0.64),\\(0.59,0.67,0.72)\end{Bmatrix}$	$\begin{Bmatrix}(0.48,0.52,0.85),\\(0.25,0.56,0.67),\\(0.31,0.43,0.74)\end{Bmatrix}$
PX_4	$\begin{Bmatrix}(0.54,0.68,0.74),\\(0.34,0.57,0.63),\\(0.46,0.63,0.72)\end{Bmatrix}$	$\begin{Bmatrix}(0.43,0.62,0.71),\\(0.54,0.68,0.79),\\(0.45,0.54,0.63)\end{Bmatrix}$
PX_5	$\begin{Bmatrix}(0.53,0.69,0.81),\\(0.64,0.72,0.76),\\(0.45,0.58,0.74)\end{Bmatrix}$	$\begin{Bmatrix}(0.34,0.53,0.76),\\(0.39,0.48,0.56),\\(0.32,0.45,0.64)\end{Bmatrix}$

	PG_3	PG_4
PX_1	$\begin{Bmatrix}(0.53,0.61,0.76),\\(0.42,0.54,0.65),\\(0.74,0.81,0.86)\end{Bmatrix}$	$\begin{Bmatrix}(0.28,0.43,0.67),\\(0.34,0.58,0.89),\\(0.63,0.75,0.83)\end{Bmatrix}$
PX_2	$\begin{Bmatrix}(0.43,0.57,0.84),\\(0.46,0.51,0.62),\\(0.37,0.43,0.57)\end{Bmatrix}$	$\begin{Bmatrix}(0.31,0.42,0.46),\\(0.54,0.65,0.74),\\(0.56,0.64,0.83)\end{Bmatrix}$
PX_3	$\begin{Bmatrix}(0.62,0.74,0.86),\\(0.29,0.56,0.69),\\(0.39,0.46,0.76)\end{Bmatrix}$	$\begin{Bmatrix}(0.73,0.76,0.82),\\(0.57,0.68,0.75),\\(0.43,0.56,0.62)\end{Bmatrix}$
PX_4	$\begin{Bmatrix}(0.63,0.84,0.89),\\(0.23,0.38,0.57),\\(0.28,0.36,0.46)\end{Bmatrix}$	$\begin{Bmatrix}(0.35,0.52,0.73),\\(0.67,0.73,0.78),\\(0.29,0.34,0.45)\end{Bmatrix}$
PX_5	$\begin{Bmatrix}(0.57,0.62,0.71),\\(0.46,0.53,0.67),\\(0.53,0.62,0.74)\end{Bmatrix}$	$\begin{Bmatrix}(0.43,0.52,0.63),\\(0.36,0.46,0.54),\\(0.48,0.52,0.63)\end{Bmatrix}$

Step 3. Construct the weight with entropy:

$$UW_1 = 0.1933, UW_2 = 0.3410, UW_3 = 0.2578, UW_4 = 0.2079.$$

Step 4. Construct the TFNNPIA and TFNNNIA (Table 3).

Table 3. The TFNNPIA and TFNNNIA

	UG_1	UG_2
TFNNPIA	$\begin{Bmatrix}(0.63,0.68,0.73),\\(0.47,0.53,0.64),\\(0.36,0.42,0.56)\end{Bmatrix}$	$\begin{Bmatrix}(0.57,0.63,0.69),\\(0.57,0.61,0.72),\\(0.36,0.42,0.54)\end{Bmatrix}$
TFNNNIA	$\begin{Bmatrix}(0.53,0.69,0.81),\\(0.64,0.72,0.76),\\(0.45,0.58,0.74)\end{Bmatrix}$	$\begin{Bmatrix}(0.34,0.53,0.76),\\(0.39,0.48,0.56),\\(0.32,0.45,0.64)\end{Bmatrix}$
	UG_3	UG_4
TFNNPIA	$\begin{Bmatrix}(0.62,0.74,0.86),\\(0.29,0.56,0.69),\\(0.39,0.46,0.76)\end{Bmatrix}$	$\begin{Bmatrix}(0.73,0.76,0.82),\\(0.57,0.68,0.75),\\(0.43,0.56,0.62)\end{Bmatrix}$
TFNNNIA	$\begin{Bmatrix}(0.43,0.57,0.84),\\(0.46,0.51,0.62),\\(0.37,0.43,0.57)\end{Bmatrix}$	$\begin{Bmatrix}(0.28,0.43,0.67),\\(0.34,0.58,0.89),\\(0.63,0.75,0.83)\end{Bmatrix}$

Step 5. Construct the $TFNNPIA\left(\xi_{ij}\right)$ and $TFNNNIA\left(\xi_{ij}\right)$ (Table 4-5).

Table 4. The $TFNNPIA\left(\xi_{ij}\right)$

Alternatives	UG_1	UG_2	UG_3	UG_4
UX_1	0.6941	1.0000	0.5346	0.6312
UX_2	1.0000	0.8662	0.6236	0.6167
UX_3	0.6605	0.6307	1.0000	1.0000
UX_4	0.8942	0.4872	0.6529	0.6599
UX_5	0.6933	0.5532	0.7780	0.6570

Table 5. The $TFNNNIA\left(\xi_{ij}\right)$

Alternatives	UG_1	UG_2	UG_3	UG_4
UX_1	0.5494	0.4499	0.5343	1.0000

UX_2	0.9995	0.5817	1.0000	0.8297
UX_3	0.5652	0.4712	0.4303	0.5056
UX_4	0.6599	0.6599	0.9055	0.5332
UX_5	1.0000	1.0000	0.6182	0.6045

Step 6. Construct the $TFNNGRD\left(\xi_i^+\right)$ and $TFNNGRD\left(\xi_i^-\right)$ (Table 6):

Table 6. $TFNNGRD\left(\xi_i^+\right)$ and $TFNNGRD\left(\xi_i^-\right)$

	$TFNNGRD\left(\xi_i^+\right)$	$TFNNGRD\left(\xi_i^-\right)$
UX_1	0.7442	0.6053
UX_2	0.7777	0.8219
UX_3	0.8085	0.4860
UX_4	0.6445	0.6969
UX_5	0.6598	0.8193

Step 7. Put forward the $TFNNRRDV\left(\xi_i\right)$ (Table 7).

Table 7. The $TFNNRRDV\left(\xi_i\right)$

	$TFNNRRDV\left(\xi_i\right)$	Order
UX_1	0.5515	2
UX_2	0.4862	3
UX_3	0.6246	1
UX_4	0.4805	4
UX_5	0.4461	5

Step 8. From $TFNNRRDV\left(\xi_i\right)$, the order is constructed: $UX_3 > UX_1 > UX_2 > UX_4 > UX_5$ and UX_3 is the best internally cured HSC.

4.2. Comparative analysis

The TFNN-GRA approach is compared with TFNNWA approach [33], TFNNWG approach [33], SVTNDPNBM approach [40], TFNN-CE technique[41], TFNN-VIKOR technique[42], TFNN-MABAC technique[37] and TFN-EDAS approach [43]. The order of these approaches is constructed in Table 8 and Figure 2.

Table 8. Order for different approaches

	order
TFNNWA technique [33]	$UX_3 > UX_1 > UX_2 > UX_4 > UX_5$
TFNNWG technique [33]	$UX_3 > UX_1 > UX_4 > UX_2 > UX_5$
SVTNDPNBM technique [40]	$UX_3 > UX_1 > UX_4 > UX_2 > UX_5$
TFNN-CE technique[41]	$UX_3 > UX_1 > UX_2 > UX_4 > UX_5$
TFNN-VIKOR technique[42]	$UX_3 > UX_1 > UX_2 > UX_4 > UX_5$
TFNN-MABAC technique[37]	$UX_3 > UX_1 > UX_2 > UX_4 > UX_5$
TFN-EDAS technique [43]	$UX_3 > UX_1 > UX_2 > UX_4 > UX_5$
TFNN-GRA technique	$UX_3 > UX_1 > UX_2 > UX_4 > UX_5$

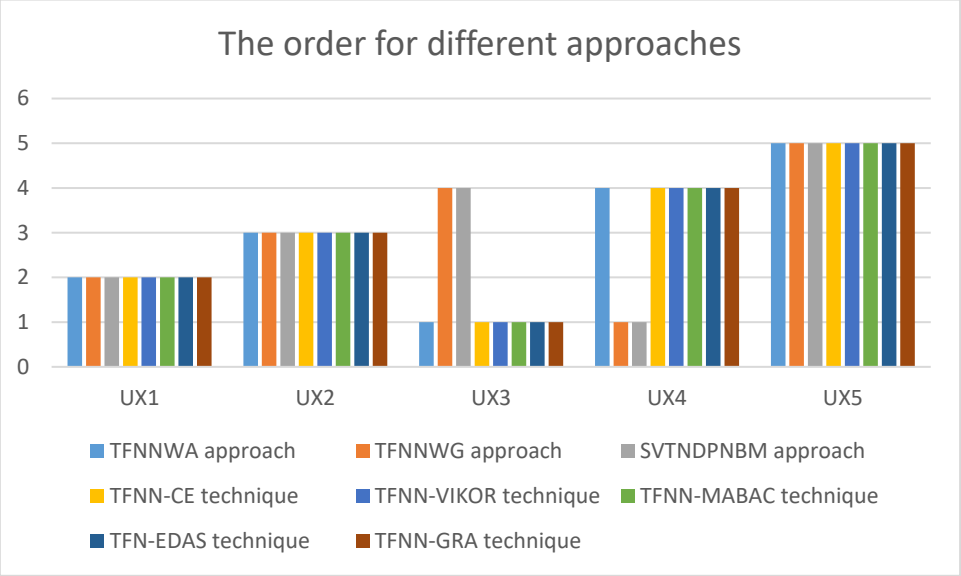

Figure 2. Order for different techniques

Based on the WS coefficients [44, 45], the WS coefficient between the existing techniques and the newly developed TFNN-GRA technique are constructed: 1.0000, 0.9236, 0.9236, 1.0000, 1.0000, 1.0000, and 1.0000, respectively. From this analysis, it is evident that both models identify the same optimal and worst internally cured HSC, confirming the effectiveness of the TFNN-GRA technique.

The key differences between the newly developed TFNN-GRA technique and the existing TFNN-GRA technique [39] are as follows:

(1) **Weight Determination**: The newly developed TFNN-GRA uses objective weights, while the existing TFNN-GRA[39] employs subjective weights.

(2) **Weight Derivation Method**: The new TFNN-GRA utilizes entropy, score, and accuracy functions to derive objective weights, whereas the existing TFNN-GRA[39] relies on subjective weights without applying a specific weighting method.

(3) **Distance Metric**: The new TFNN-GRA applies a mixed distance measure to calculate the GRC and GRD, while TFNN-GRA [39] uses the Hamming distance for these calculations.

One limitation of the newly developed TFNN-GRA technique is that it fails to incorporate consensus measures and prospect theory for the performance evaluation of internally cured HSC.

5. Conclusion

The curing conditions of concrete can significantly affect its early strength development. Inadequate early curing of high-performance concrete with a low water-cement ratio not only results in increased volume shrinkage and early cracking due to self-drying but also severely reduces early strength because of internal water shortages and a slower hydration reaction rate. In response, most domestic scholars and engineers have focused on improving the early hydration and strength of concrete by increasing the curing temperature and humidity of the external environment. However, there have been no reports in China on producing self-curing concrete that is less sensitive to external curing conditions by incorporating self-curing agents. Exploring the production of self-curing high-performance concrete is of great significance. It can improve construction conditions, reduce concrete curing costs, and expand the application fields and scope of high-performance concrete. Additionally, it offers a new approach to minimizing shrinkage in high-performance concrete. The performance evaluation of internally cured HSC is treated as a MADM problem. In this study, the TFNN-GRA technique is proposed under the framework of TFNSs. The entropy method is applied to derive the weight under TFNSs. Following this, the GRA technique is adapted to work with TFNSs, and the TFNN-GRA process for MADM is outlined step by step. Finally, numerical example is constructed to demonstrate the performance evaluation of internally cured HSC, and comparative studies are validated the TFNN-GRA technique.

References

[1] M. Lopez, L.F. Kahn, K.E. Kurtis, Effect of internally stored water on creep of high-performance concrete, Aci Materials Journal, 105 (2008) 265-273.

[2] W.J. Weiss, P. Lura, Special section on advances in internally cured concrete introduction, Journal of Materials in Civil Engineering, 24 (2012) 959-960.

[3] D.J. Shen, J.L. Jiang, M.Y. Zhang, P.P. Yao, G.Q. Jiang, Tensile creep and cracking potential of high performance concrete internally cured with super absorbent polymers at early age, Construction and Building Materials, 165 (2018) 451-461.

[4] F.J. Vázquez-Rodríguez, A. Arato, D.I. Martinez-Delgado, A. Guzmán, N. Elizondo-Villarreal, R. Puente-Ornelas, E. Rodríguez, Evaluation of chloride diffusion and corrosion resistance in reinforced concrete using internal curing and shrinkage reducing admixtures, International Journal of Electrochemical Science, 13 (2018) 6027-6047.

[5] J. Zhang, X. Zheng, Q. Wang, Mixture optimization on internally cured high strength engineered cementitious composite with pre-wetted sand-like zeolite, Journal of Advanced Concrete Technology, 16 (2018) 485-497.

[6] T. Manzur, S. Rahman, T. Torsha, M.A. Noor, K.M.A. Hossain, Burnt clay brick aggregate for internal curing of concrete under adverse curing conditions, Ksce Journal of Civil Engineering, 23 (2019) 5143-5153.

[7] D.J. Shen, Z.Z. Feng, J.C. Kang, C.Y. Wen, H.F. Shi, Effect of barchip fiber on stress relaxation and cracking potential of concrete internally cured with super absorbent polymers, Construction and Building Materials, 249 (2020) 13.

[8] M. Rajczakowska, K. Habermehl-Cwirzen, H. Hedlund, A. Cwirzen, The effect of exposure on the autogenous self-healing of ordinary portland cement mortars, Materials, 12 (2019) 23.

[9] D.J. Shen, C. Liu, Z.Z. Feng, S.S. Zhu, C. Liang, Influence of ground granulated blast furnace slag on the early-age anti-cracking property of internally cured concrete, Construction and Building Materials, 223 (2019) 233-243.

[10] D.J. Shen, C. Liu, C.C. Li, X.G. Zhao, G.Q. Jiang, Influence of barchip fiber length on early-age behavior and cracking resistance of concrete internally cured with super absorbent polymers, Construction and Building Materials, 214 (2019) 219-231.

[11] A. Danish, M.A. Mosaberpanah, M.U. Salim, Robust evaluation of superabsorbent polymers as an internal curing agent in cementitious composites, Journal of Materials Science, 56 (2021) 136-172.

[12] N. Hamzah, H.M. Saman, M.H. Baghban, A.R.M. Sam, I. Faridmehr, M.N.M. Sidek, O. Benjeddou, G.F. Huseien, A review on the use of self-curing agents and its mechanism in high-performance cementitious materials, Buildings, 12 (2022) 27.

[13] T.G. Atsbha, S. Zhutovsky, Optimising internal curing parameters for autonomous curing of normal-strength concrete, Magazine of Concrete Research, 75 (2023) 888-905.

[14] Z.Z. Feng, D.J. Shen, C.Y. Wen, X.J. Tang, G.Q. Jiang, Effect of water-to-cement ratios on performance of concrete with prewetted lightweight aggregates, Journal of Materials in Civil Engineering, 35 (2023) 14.

[15] M.M. Jaberizadeh, P.A. Danoglidis, S.P. Shah, M.S. Konsta-Gdoutos, Eco-efficient cementitious composites using waste cellulose fibers: Effects on autogenous shrinkage, strength and energy absorption capacity,

Construction and Building Materials, 408 (2023) 14.

[16] Q. Wang, W.J. Huang, J. Sun, J. Zhang, Shrinkage of high-strength engineered cementitious composite with zeolite particles as internal curing agent, Advances in Cement Research, 35 (2023) 287-296.

[17] Y. Wei, W.Q. Guo, L. Ma, Y.L. Liu, B.Y. Yang, Materials, structure, and construction of a low-shrinkage uhpc overlay on concrete bridge deck, Construction and Building Materials, 406 (2023) 19.

[18] J.T. Xu, X. Qin, Y.K. Lin, C.F. Cao, J.H. Liu, Q.J. Huang, Research on performance deterioration of internally cured pavement concrete under the coupling effect of salt freeze-thaw, Polymers, 15 (2023) 25.

[19] Y.T. Zhang, J.H. Lin, Z.W. Fan, X.Y. Zhu, Durability of internally cured concrete with silicon-aluminum based fine lightweight aggregate exposed to combined sulfate and wetting-drying attack, Materials and Structures, 56 (2023) 14.

[20] K. Zhang, Y.J. Xie, S.A. Noorkhah, M. Imeni, S.K. Das, Neutrosophic management evaluation of insurance companies by a hybrid todim-bsc method: A case study in private insurance companies, Management Decision, 61 (2023) 363-381.

[21] Z.Y. Wang, Q. Cai, J.P. Lu, G.W. Wei, Sustainable supplier selection by using dual probabilistic linguistic edas and itara method, Journal of Intelligent & Fuzzy Systems, 44 (2023) 9495-9512.

[22] T. Senapati, G.Y. Chen, R. Mesiar, R.R. Yager, Intuitionistic fuzzy geometric aggregation operators in the framework of aczel-alsina triangular norms and their application to multiple attribute decision making, Expert Systems with Applications, 212 (2023) 15.

[23] T. Senapati, An aczel-alsina aggregation-based outranking method for multiple attribute decision-making using single-valued neutrosophic numbers, Complex & Intelligent Systems, (2023) 15.

[24] P. Rani, S.M. Chen, A.R. Mishra, Multiple attribute decision making based on mairca, standard deviation-based method, and pythagorean fuzzy sets, Information Sciences, 644 (2023) 15.

[25] V. Ulucay, Q-neutrosophic soft graphs in operations management and communication network, Soft Computing, 25 (2021) 8441-8459.

[26] D. Stanujkic, D. Karabasevic, G. Popovic, F. Smarandache, E.K. Zavadskas, I. Meidute-Kavaliauskiene, Multiple-criteria decision-making based on the use of single-valued neutrosophic sets and similarity measures, Economic Computation and Economic Cybernetics Studies and Research, 55 (2021) 5-22.

[27] L.A. Zadeh, Fuzzy sets, Information and Control, 8 (1965) 338-353.

[28] F. Smarandache, Neutrosophic probability, set, and logic, proquest information & learning, Ann Arbor, Michigan, USA, 105 (1998) 118-123.

[29] F. Smarandache, Neutrosophy: Neutrosophic probability, set, and logic: Analytic synthesis & synthetic analysis, American Research Press, 1998.

[30] F. Smarandache, A unifying field in logics: Neutrosophic logic. Neutrosophy, neutrosophic set, neutrosophic probability: Neutrsophic logic, Infinite Study, 2005.

[31] H.Y. Zhang, J.Q. Wang, X.H. Chen, An outranking approach for multi-criteria decision-making problems with interval-valued neutrosophic sets, Neural Computing & Applications, 27 (2016) 615-627.

[32] P.K. Singh, Interval-valued neutrosophic graph representation of concept lattice and its ()-decomposition,

Arabian Journal for Science and Engineering, 43 (2018) 723-740.

[33] P. Biswas, S. Pramanik, B.C. Giri, Aggregation of triangular fuzzy neutrosophic set information and its application to multi-attribute decision making, Neutrosophic Sets and Systems, 12 (2016) 20-40.

[34] J.L. Deng, Introduction to grey system, The Journal of Grey System, 1 (1989) 1-24.

[35] G. Wei, New method of grey relational analysis to multiple attribute decision making with intervals, Systems Engineering and Electronics, 28 (2006) 1358-1359+1383.

[36] G. Wei, H. Yao, New method of grey related analysis to multiple attribute decision making problem with interval numbers, Statistics and Decision, 2006 (2006) 131.

[37] I. Irvanizam, N.N. Zi, R. Zuhra, A. Amrusi, H. Sofyan, An extended mabac method based on triangular fuzzy neutrosophic numbers for multiple-criteria group decision making problems, Axioms, 9 (2020) 18.

[38] C.E. Shannon, A mathematical theory of communication, Bell System Technical Journal, 27 (1948) 379-423.

[39] B. Xie, Modified gra methodology for madm under triangular fuzzy neutrosophic sets and applications to blended teaching effect evaluation of college english courses, Soft Computing, (2023) https://doi.org/10.1007/s00500-00023-08891-00506.

[40] J.P. Fan, X.F. Jia, M.Q. Wu, Green supplier selection based on dombi prioritized bonferroni mean operator with single-valued triangular neutrosophic sets, International Journal of Computational Intelligence Systems, 12 (2019) 1091-1101.

[41] L. Li, Cross-entropy method for efficiency evaluation of integrated development of agriculture and tourism to promote rural revitalization under the triangular fuzzy neutrosophic sets, Journal of Intelligent & Fuzzy Systems, 44 (2023) 6151-6161.

[42] J. Wang, G.W. Wei, M. Lu, An extended vikor method for multiple criteria group decision making with triangular fuzzy neutrosophic numbers, Symmetry-Basel, 10 (2018) 15.

[43] J.P. Fan, X.F. Jia, M.Q. Wu, A new multi-criteria group decision model based on single-valued triangular neutrosophic sets and edas method, Journal of Intelligent & Fuzzy Systems, 38 (2020) 2089-2102.

[44] W. Salabun, K. Urbaniak, A new coefficient of rankings similarity in decision-making problems, in: 20th Annual International Conference on Computational Science (ICCS), Springer International Publishing Ag, Amsterdam, NETHERLANDS, 2020, pp. 632-645.

[45] W. Sałabun, J. Wątróbski, A. Shekhovtsov, Are mcda methods benchmarkable? A comparative study of topsis, vikor, copras, and promethee ii methods, Symmetry, 12 (2020) 1549.

Received: June 28, 2024. Accepted: Oct 12, 2024